Environ Geol (2006) 49: 696–707
DOI 10.1007/s00254-005-0108-x

ORIGINAL ARTICLE

He Keqiang
Wang Sijing

Double-parameter threshold and its formation mechanism of the colluvial landslide: Xintan landslide, China

Received: 7 March 2005
Accepted: 20 September 2005
Published online: 9 November 2005

H. Keqiang (✉)
Department of Civil Engineering, Qingdao Technological University, Qingdao, Shandong 266033, PR China
E-mail: keqianghe@163.com
Tel.: +86-532-85071758
Fax: +86-532-85071798

W. Sijing
Institute of Geology and Geophysics, Chinese Academy of Sciences, Beijing 100029, PR China

Abstract Data compiled from monitoring the displacement resulting from the Xintan landslide in China was analyzed. The stability of the demonstrated colluvial slope has a close correlation with two parameters, the velocity of the displacement and the angle of the surface vector. The stability trend can be described and evaluated by both the velocity of the displacement and the vector angles. The displacement vector angle, for which there is no substitute, serves as an explicit criterion for the stability of the slope, hence it is significant in the prediction of the catastrophic movement of landslides. A systematic analysis of the features of the vector angles of the surface displacement space and time was performed. The evolving mechanism of space-time and the characteristics of the displacement vector angles were deduced. On the basis of these deductions and by using principles of statistics, the double-parameter threshold for forecasting the stability of the colluvial slopes was established. According to the double-parameter threshold, a calculation and evaluation of stability was completed in terms of the monitoring data of the F-series of points on the Xintan slope. The forecast results coincided with the destabilized timetable, thus demonstrating that the double-parameter criterion has, to a certain extent, precision and practical application for forecasting of landslides.

Keywords Colluvial slope · Surface displacement vector angle · Displacement velocity · Space-time characteristics · Double-parameter threshold · Xintan landslide · China slope stability

Introduction

Long-term quantitative monitoring of slope surface displacements and analysis of the displacement data are two very important means of medium- and short-term landslide forecasting, and also serve as a basis for analyzing the sliding phenomena of slopes, particularly for the colluvial landslides. Colluvial landslides refer to the landslides that occurred in the Quaternary System or in the relative loose accumulative stratum (Adib 2000). They are generally characterized by loose composition, large porosity and strong permeability due to the specific composition of the sliding mass. Because of complex boundaries, dynamic changes, and specific composition of sliding mass, colluvial landslides have deformation and slippage properties which are different from other types of landslides, such as rock-mass landslide (Brand 1981; Mair 1993). A key point in landslide research is how to fully analyze deformation data to make precise predictions so that effective prevention measures may be taken (Chen and Chan 1984; Savage 1986). The time-sequence analysis method proposed by the famous Japanese scholar Saito has great success in the prediction of some small-scale soil landslides, but this method has often proved ineffective in the large-scale colluvial landslides (Santian 1980; Wang 1999). The main reason

for discrepancies, in our opinion, is that the Saito method uses only one responding parameter, displacement or displacement velocity, as the basis for analysis. For the small-scale homogeneous and isotropic soil slope with simple boundaries, the stress and deformation field of the slope is fairly well distributed. So, the pattern and magnitude of the displacement or the displacement velocity can generally reflect the stage of slide evolution and the stability state. In this case, the parameter of the displacement or the displacement velocity can be used for prediction of landslide effectively. But for the large-scale anisotropic colluvial landslide with complex boundaries, the displacement, or the displacement velocity shows variations due to the factors such as the complex boundaries, the anisotropic composition of the colluvial mass, the changing groundwater level or some external load, etc., and the displacement–time curve is generally a random wave. Therefore, the threshold and pattern of displacement velocity of colluvial landslides differ in different types and shapes of slopes and varies also according to the geological composition, and the critical displacement velocity is very difficult to determine for the type of landslides. Because of these variations in the displacement velocity, the stability of the colluvial slope cannot easily be accurately evaluated by considering only displacement velocity.

In order to overcome the deficiency of Saito method which uses only single parameter, another important displacement parameter, the displacement vector angle, which can reflect the dynamic condition and the sliding mechanism of the colluvial slopes and which cannot be substituted by the parameter of displacement or displacement velocity, was applied in establishing the double-parameter threshold for prediction of colluvial landslides.

Based on an analysis of displacement data of a typical colluvial landslide: the Xintan landslide, China, a statistical treatment of surface displacement data is provided that is based on the evolving mechanism of sliding. Two displacement parameters are used to describe these mechanisms and thus serve as key diagnostics for time series analysis. A double-parameter prediction threshold for a colluvial landslide is presented. The double-parameter prediction result for the colluvial landslide: Xintan landslide, China, shows that the double-parameter threshold can be used for prediction of the colluvial landslides.

The surface displacement vector angle and its dynamic features in different deformation stages

The relationship between surface displacements and displacement angles

The displacement monitoring values of a slope should be a vector, which includes both magnitude and direction. The displacement magnitude is generally represented by the monitored displacement value, and the displacement direction can be described by the parameter of the displacement vector angle. The two parameters of displacement are equally important in evaluating colluvial landslides.

The surface displacement vector angle of the slope is the angle of the surface displacement vectors, which is defined as the surface displacement vector angle = *arctan* (vertical displacement/horizontal displacement).

Suppose $x(t_{i+1})$ and $x(t_i)$ represent the horizontal displacements at time t_i and t_{i+1}; $y(t_{i+1})$ and $y(t_i)$ are the vertical displacements at time t_i and t_{i+1}; $\vec{V}_i, \vec{V}_{i+1}$ stand for the surface displacement vectors at time t_i and t_{i+1}; $\Delta\vec{V}$ the surface displacement vector during the period of $(t_{i+1} - t_i)$. The surface displacement vector angles $\theta\ (t_{i+1})$, $\theta\ (t_i)$ and $\Delta\ \theta\ (\Delta t)$ at different times can be defined as follows:

$$\begin{aligned}\theta(t_i) &= \arctan(y(t_i)/x(t_i))\\ \theta(t_{i+1}) &= \arctan(y(t_{i+1})/x(t_{i+1}))\\ \Delta\theta(\Delta t) &= \arctan[(y(t_{i+1}) - y(t_i))/(x(t_{i+1}) - x(t_i))]\end{aligned} \quad (1)$$

Surface displacement vectors and their angles in different area of the colluvial landslide are shown in Fig. 1 with different compositions of vertical displacements and horizontal displacements.

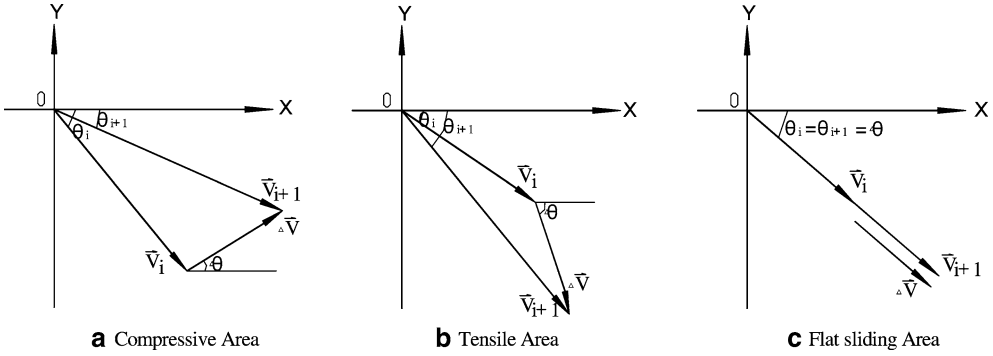

Fig. 1 Displacements vector angle in the area of compression, extension and lateral movement

The space distribution features of the surface displacement vector angles of different types of sliding zones

Due to the lack of symmetry of the sliding slope and the different stress conditions in certain zones, difference in deformation occurred during sliding. The sliding portion of the slope can be classified as the active sliding zones, the passive sliding zones and the flat sliding zone (Fig. 2).

The active sliding zone is the dynamic zone which controls the catastrophic movement of landslides. The passive sliding zone is more stable and is also the most resistant to movement. When the active sliding zone meets the resistance of the passive sliding zone, a resistant area to sliding is formed. The sliding body meets resistance and enters a state of compressive stress. The deformation modulus (Es) increases. With adjustment of the slope stress, the effective principal stress in the compressive zones of the slope gradually increases, but the least effective principal stress has little change. This leads to an increase of the shearing stress in the slope. When the shearing stress exceeds the shearing strength of the slope, the slope will no longer be in equilibrium, and a plastic shearing zone forms inside. When local shearing zone increases with continuing stress, a continuous plastic sliding plane may form (Chen and Zhang 1986). The slope moves along the shearing zone that has the least resistance, and the movement of the colluvial slope causes the surface displacement vector angles to be rotated in the direction of the ground surface. The displacement vector angles decreases, and a compressive shearing zone appears in the slope (Figs. 1, 2).

When the passive sliding zone is located behind an active sliding zone, the active sliding zone is usually in a state of tension, due to the movement of the active zone. The compressive stress is suddenly lost. The maximum principal stress of the slope varies with the gradual decrease of the least principal stress. This leads to the gradual increase of the shearing stress in the slope. In this case, the slope leaves a state of limited plastic equilibrium and forms tensile shearing planes at high angles. Under the action of the tensile stress, the slope will slide along the plane of shearing, leading to an increase in the surface displacement vector angle (Figs. 1, 2).

In the flat sliding zone, the slope slides along the planar plane and cannot meet any resistance in its movement, so variation patterns of the displacement vector angle are closely controlled and affected by the variation of the inclination of the sliding plane. For landslides with a relatively planar sliding plane, the displacement vector angles basically do not change, but for a curved-sliding plane, the displacement vector angles decrease (Figs. 1, 2).

The dynamic features of the displacement vector angles in different deformation stages

The different stability zones of a slope are the comprehensive reflection of its internal and external forces, and they may generally be defined spatially. Structure of sliding mass, physical and mechanical parameters of the sliding mass, and magnitudes of stresses within it, all affect stability. The combined action of these factors is reflected in the dynamic features of the slope's stability at any stage. The factor of safety, which is defined as the ratio of resistance force to sliding force along the sliding plane is calculated by means of the Sarma method (Wang 1999).

Based on previous studies on the dynamic features of the Xintan landslide in China (Wang et al. 1988), the basic displacement features of a large-scale colluvial landslide are described in Table 1.

The basic geology and landform conditions of the Xintan slope and its surface displacement features

The basic geology and landform situation

The Xintan landslide, 27 km upriver from the Sandouping Dam of the three Gorges Project, is in Xintan County on the north bank of the Yangtze River. This colluvial landslide, which occurred on June 12, 1985,

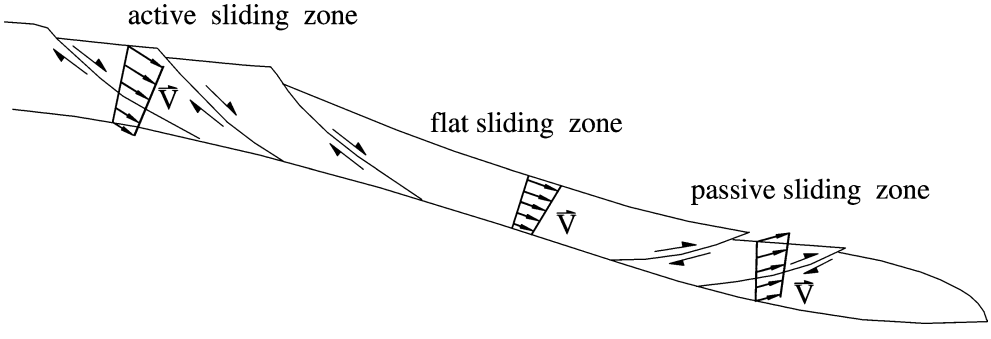

Fig. 2 Displacement vectors in different sliding portions of the colluvial slope

Table 1 The dynamic stability features of Xintan landslides

Sliding stage		Stability state	Factor of safety (k)	Topography features	Slope's displacement constitution
I Creep stage (before 1979)		No sliding plane (zone); factor of safety $(k) > 1$; slope is in stable state	1.10–1.05	Existing intermittent extension cracks on the slope	Only creep deformation
II Compressive deforming stage (1979–1982)		Stress field starts to be adjusted as slope moves; factor of safety $(k) \geqslant 1$; displacement is relatively small in this stage	1.05–1.00	Extension fissures have been developed into continuous ones; there exist fissures on both sides of slope	Surface creep deformation and compressive deformation
III Overall sliding stage (1983–1985)	III 1 Primary sliding stage	Slope's displacement is transformed into an overall trend of deformation; active sliding plane has developed into a continuous one, factor of safety $(k) \leqslant 1$; slope is in unstable state	1.00–0.90	The lower part of the toe region bulges and rotates forward; normal fault scarp appears in head and upper section	Compressive deformation of sliding mass and overall sliding deformation
	III 2 Sliding stage	Sliding plane formed completely; factor of safety $(k) < 1$; overall landslide will take place	< 0.90	Front surface bulges increase; scale of subsidence in upper section also increases	Overall sliding deformation
IV Consolidation stage (1986–present)		After sliding, the slope's center of gravity is lowered; factor of safety $(k) > 1$; slope is in stable state	> 1.10	Having almost all topographic features of landslides	Compressive deformation caused by consolidation

had a volume of 3.0×10^7 m^3. The landmass was oriented roughly from north to south, with a length of about 2 km and an area of about 1.1 km^2. The altitude of the back section of this slope is about 900 m asl. The landslide extends to the south bank of the Yangtze River at an altitude of about 65 m asl with an average gradient of about 23°. The thickness of the colluvial body is 30–40 m, with a maximum thickness of 86 m, which increases from east to west. Due to its origin, the slope can be divided into two types: colluvial deposit and alluvial material (Fig. 3) (Wang 1999).

Two steep ridges exist in the middle of the slope (Fig. 4). One steep ridge is in the front margin of the Jiangjiapo slope and has an altitude of about 500–600 m asl. Its orientation is 30° from north to east; its height is about 40–60 m; and its gradient is about 50–60°. This steep ridge divides the slope into two sections: the back section (Jiangjiapo section) and the front section (Xintan section). Another steep ridge is in the front margin of Maojiayuan with an altitude of 270–330 m asl, and a trend of 75° from north to east. This steep ridge divides the Xintan slope into two sections: the Maojiayuan and the front slope (Liu 1988). A typical geological cross-section of the slide is shown in Fig. 4.

The monitoring system and its displacement features in different evolving stages

On the basis of the geological survey and the evolving stage of deformation of the slope, visual line method, leveling survey method, front intersection method and trigonometric method were chosen for monitoring the three-dimensional displacements of Xintan landslide. The monitoring system was composed of 5 monitoring lines, 15 observation points and 6 controlling points. Using the method of visual line and the leveling survey method, respectively, the horizontal displacements and the vertical displacements were monitored respectively by means of theodolite (WILDT3) and leveling instrument (N3). Using the front intersection method and the trigonometric leveling method, the three-dimensional displacements of monitoring points of F1–F8 were monitored by means of the theodolite.

Monitoring of the Xintan slope began in November 1977. In the early days of observation, only four monitoring lines parallel to the Yangtze River were set up. With the development of slope deformation, additional monitoring points F1–F8 were installed on the back section on July 2, 1984 (Chen and Wang 1992) (Fig. 3).

According to Wang's research results (Wang 1999), the Xintan landslide was the result of long-term deformation and development of the Jiangjiapo section of the slope. The development period can be divided into three stages: (1) a freer sliding stage (before May 1983); (2) the overall sliding stage (from May 1983 to June 1985); (3)

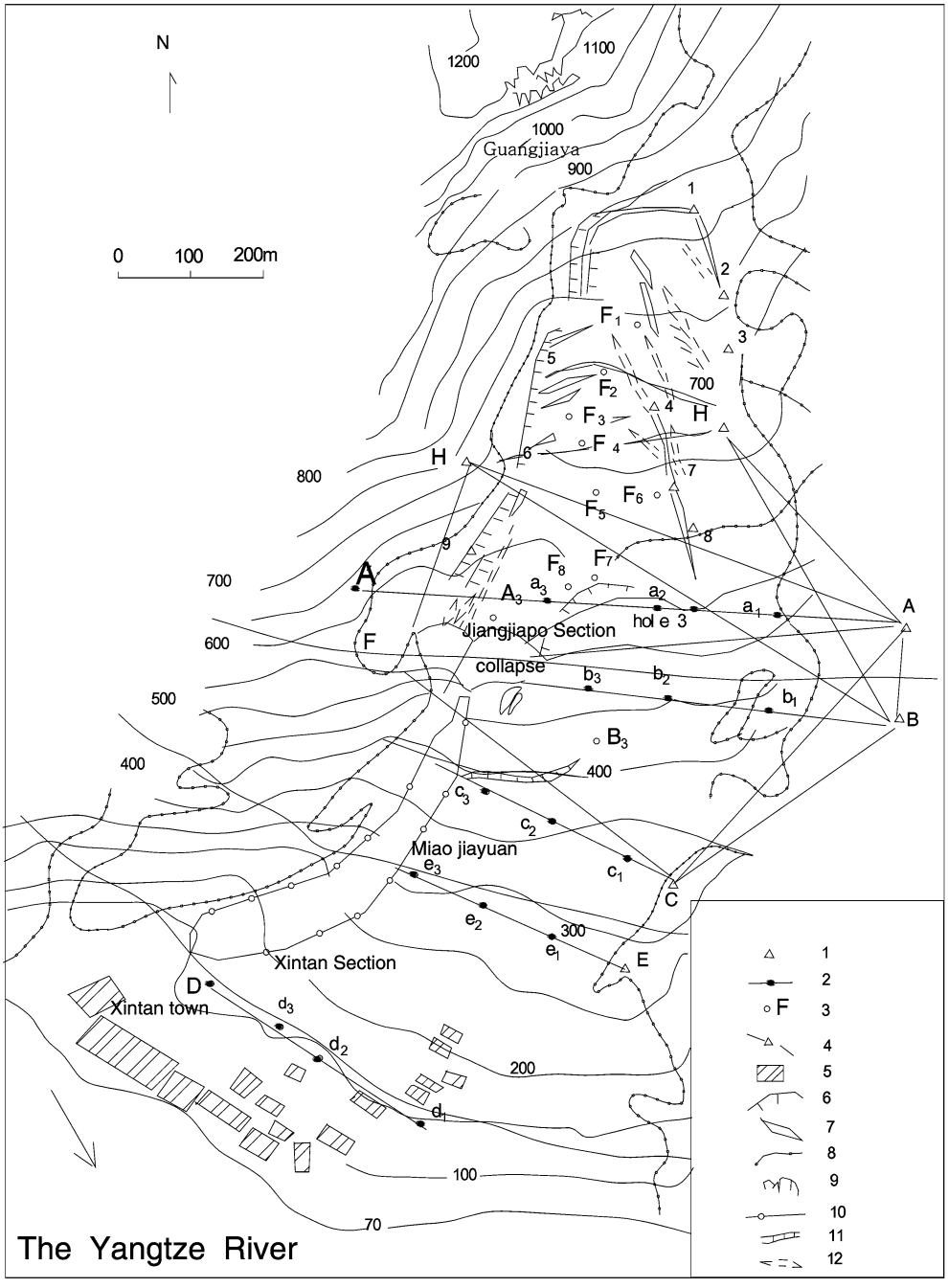

Fig. 3 Monitoring points and lines for displacement of Xintan landslide (Wang 1999)

1.Control monitoring points; 2.Monitoring lines and the points;
3.Monitoring points for displacement; 4.Simple monitoring points;
5.Residential area; 6.Cliff of falling rock-mass; 7.The tensile fissures;
8.Boundary line between Quaternary system and bedrock; 9. Cliff;
10.Boundary line of small scale slide before landslide;
11.Bulging area; 12.New ground fissures.

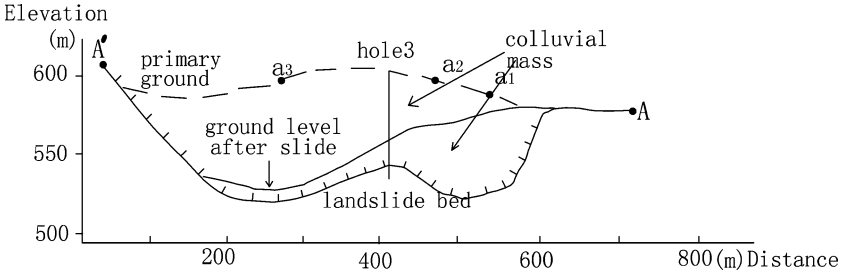

Fig. 4 A typical geological cross-section of the Xintan landslide

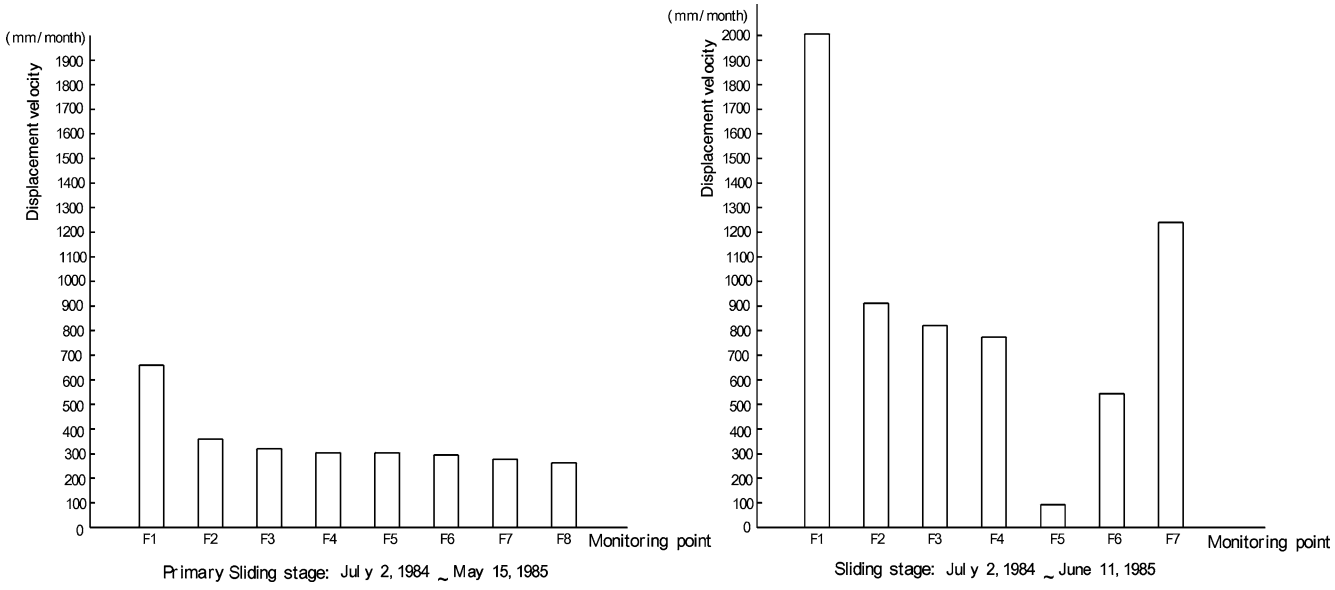

Fig. 5 Displacement velocities of primary sliding stage and sliding stage

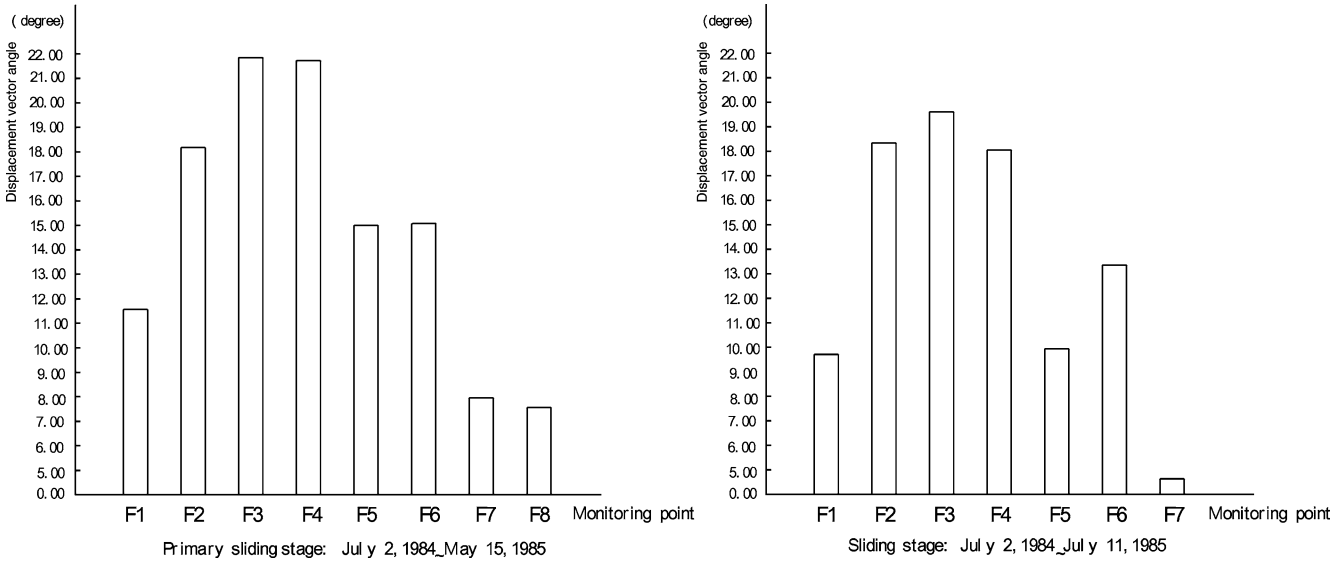

Fig. 6 Displacement vector angles of primary sliding stage and sliding stage

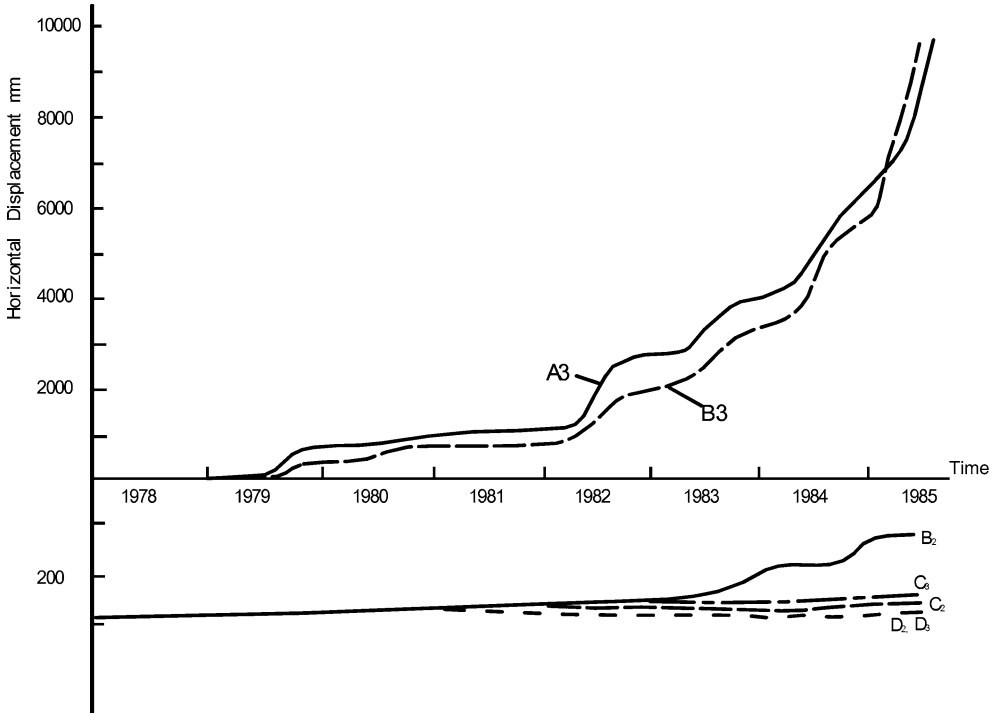

Fig. 7 Deformation–time curves of monitoring points on Xintan slope (Wang 1999)

Table 2 The displacements of monitoring points d2, B3 at different time periods (unit: mm)

Year	Month	Points			
		d2		B3	
		Horizontal displacements	Vertical displacements	Horizontal displacements	Vertical displacements
1978	March	−0.70	+0.40	+20.50	−0.50
	May	−0.40	−1.80	+8.30	−5.70
	July	−0.10	−1.30	+31.70	−11.20
	September	+0.10	−1.30	+14.50	−4.40
	November	−0.70	+0.40	+2.80	−1.00
1979	January	0.00	+0.60	+11.60	−3.40
	March	−1.00	+1.00	+8.80	−1.60
	May	−0.60	−0.30	+6.20	−3.20
	July	1.10	−0.80	+22.00	−8.20
	September	+0.10	−0.90	+175.60	−78.00
	November	−1.20	−1.80	+102.50	−35.70
1980	June	−1.00	−3.20	+66.90	−23.10
	August	−0.70	−5.40	+117.00	−66.00
	October	−1.70	−4.40	+101.70	−43.80
	December	−2.20	−1.50	+33.80	−10.30
1981	February	−1.20	−1.00	+15.20	−4.90
	April	−2.70	−3.80	+23.70	−3.80
	July	−2.70	−4.60	+25.40	−5.40
	September	−3.60	−3.60	+28.90	−10.90
	December	−3.10	−2.50	+15.00	−5.30
1982	February	−4.40	−2.00	+8.50	−4.80
	May	−4.00	−4.10	+234.10	−64.20
	August	−4.00	−3.20	–	–
	October	−3.90	−3.92	–	–
	December	−3.70	−4.30	–	–
1983	January	−3.50	−2.93	–	–
	April	−8.10	−3.57	–	–

Table 3 Displacements, velocities and vector angles of monitoring points d2, B3 at different time periods

Year	Month	Points					
		d2			B3		
		Displacements (mm)	Velocities (mm/month)	Vector angles (°)	Displacements (mm)	Velocities (mm/month)	Vector angles (°)
1978	March	0.8062	0.8062	−29.74	20.5061	20.5061	−1.40
	May	1.7804	0.8902	51.84	29.4598	14.7299	−12.15
	July	2.9547	1.4773	66.04	62.9524	31.4762	−16.05
	September	4.1485	2.0742	74.62	78.1040	39.0520	−16.21
	November	4.0249	2.0125	63.43	81.0721	40.5360	−16.33
1979	January	3.4986	1.7493	59.04	93.1601	46.5800	−16.33
	March	3.4409	1.7205	35.54	102.0592	51.0296	−15.81
	May	4.1049	2.0524	34.08	108.9053	54.4526	−16.54
	July	3.8601	1.9300	53.43	132.3390	66.1695	−17.23
	September	4.5651	2.2825	61.19	323.9442	161.9721	−21.21
	November	6.7231	3.3615	59.62	432.4334	216.2167	−20.71
1980	June	10.0180	1.4311	63.95	503.1838	71.8834	−20.47
	August	15.2765	7.6382	70.50	636.2221	318.1110	−22.36
	October	19.9920	9.9960	70.11	746.9402	373.4701	−22.50
	December	22.2056	11.1028	66.09	782.1166	391.0583	−22.25
1981	February	23.6163	11.8082	64.41	798.0412	399.0206	−22.16
	April	28.2209	14.1105	62.80	821.4420	410.7210	−21.78
	July	33.5477	11.1826	62.29	847.0438	282.3479	−21.48
	September	38.4387	19.2193	60.03	877.9280	438.9640	−21.45
	December	42.1774	14.0591	58.08	893.8274	297.9425	−21.42
1982	February	46.2788	23.1394	54.76	903.4942	451.7471	−21.50
	May	51.9432	17.3144	53.77	1145.1294	381.7098	−20.20
	August	56.9043	18.9681	52.43	–	–	–
	October	62.3933	31.1966	51.78	–	–	–
	December	68.0611	34.0305	51.57	–	–	–
1983	January	72.5376	36.2688	50.85	–	–	–
	April	80.5211	26.8404	47.98	–	–	–

the stabilized stage (after June 1985). In the first stage, the deformation of the slope originated in the front and moved toward the rear. The creeping deformation period, which is defined as the average displacement per month <10 mm, occurred before August 1979. The slowly compressing deformation period, which is defined as 10 mm $\leq$ the average displacement per month <30 mm, was from August 1979 to August 1982. The deformation development period, which is defined as 30 mm $\leq$ the average displacement per month <50 mm, was from September 1982 to April 1983. The second stage, May 1983 to June 1985, can be further divided into the developed deformation period, which is defined as 50 mm $\leq$ the average displacement per month <100 mm, which occurred from May 1983 to May 1985 and the sharp deformation period, in which the average displacement per month ≥ 100 mm, which occurred from mid-May 1985 to June 12, 1985 (Fig. 7). In the third stage, after June 12, 1985, the Xintan slope was stabilized by a natural way after the slide. There was little movement of Xintan slope after June 1985.

The monitoring points B3 and the F-series points are in the Jiangjiapo section of Xintan slope, which was unsteady and a sliding zone. The displacement of the monitoring points on the portion was generally large and active. The stability of the Jiangjiapo section represents the stability of the whole Xintan slope. In contrast, the Xintan section was the relatively stable region and the points C, D and E in the Xintan section are generally small and passive. According to the distribution of the monitoring points, to complete the comparison for the displacement between the two sections, the representational points d2, B3 and F are selected as analytical points. A statistical analysis on the displacement monitoring data of points d2 and B3 from March 1978 to April 1983 (Tables 2, 3) and F-series points from July 2, 1984 to June 11, 1985 (Tables 4, 5, 6) was carried out. Thus, the displacement velocities and the displacement vector angles of every monitoring point in both periods were calculated, respectively (Figs 5 and 6).

The principle for trend displacement statistical analysis and the double-parameter threshold

A brief description of Saito's prediction method of landslide

According to lot of experiments and observations, Saito obtained an empirical correlation between the time to

Table 4 Displacements of F-series points (unit: mm)

Time	Points							
	F1	F2	F3	F4	F5	F6	F7	F8
July 2, 1984–October 24, 1984	2945.0	1535.2	1375.2	1295.4	1325.8	1261.3	1145.7	1185.7
July 2, 1984–November 21, 1984	3714.8	1672.5	1764.2	1675.9	1707.6	1604.2	1531.4	1454.9
July 2, 1984–May 15, 1985	6898.9	3752.1	3339.6	3172.9	3172.9	3070.5	2897.7	2750.3
July 2, 1984–June 11, 1985	22674.4	10296.4	9285.0	8753.1	1042.9	6144.9	14002.1	–

Table 5 Displacement velocities of points F1–F8 (unit: mm/month)

Time	Points							
	F1	F2	F3	F4	F5	F6	F7	F8
July 2, 1984–October 24, 1984	788.84	411.21	368.36	346.98	355.13	337.85	306.88	317.60
July 2, 1984–November 21,1984	801.76	360.97	380.76	361.71	368.55	346.23	330.52	314.01
July 2, 1984–May 15, 1985	661.24	359.63	320.09	304.11	304.11	294.30	277.73	263.61
July 2, 1984–June 11, 1985	2006.58	911.19	821.68	774.61	92.29	543.80	1239.12	–

Table 6 Displacement vector angles of the F-series points (unit: degree)

Time	Points							
	F1	F2	F3	F4	F5	F6	F7	F8
July 2, 1984–October 24, 1984	9.667	18.026	21.891	21.765	15.119	15.239	8.026	7.348
July 2, 1984–November 21, 1984	10.695	18.312	21.894	21.729	15.070	15.421	8.270	7.700
July 2, 1984–May 15, 1985	11.567	18.178	21.819	21.712	15.058	15.126	7.956	7.549
July 2, 1984–June 11, 1985	9.712	18.341	19.607	18.049	9.930	13.351	4.624	–

Table 7 The evaluation results of trend velocity of F-series points (July 2, 1984–June 11, 1985)

Parameters	Points							
	F1	F2	F3	F4	F5	F6	F7	F8
$\gamma_i\,(v\,)$	0.8252	0.7305	0.9331	0.9869	0.9623	0.8900	1.1962	0.7004
$\gamma_d\,(v\,)$	1.0069	1.0069	1.0069	1.0069	1.0069	1.0069	1.0069	1.0069
Evaluation results	T	T	T	T	T	T	F	T
$(\gamma_d-\gamma)/\gamma_{d(\%)}$	18.04	27.45	7.33	1.99	4.43	11.61	–	30.44

T, with trend shift; F, without trend shift

Table 8 The evaluation results of the trend vector angle of F-series points (July 2, 1984–June 11, 1985)

Parameters	Points							
	F1	F2	F3	F4	F5	F6	F7	F8
$\gamma_{\ i}\,(\theta\,)$	1.0714	1.0126	0.6382	0.6582	0.6604	0.5876	0.6233	0.6757
$\gamma_{\ d}\,(\theta\,)$	0.7418	0.7418	0.7418	0.7418	0.7418	0.7418	0.7418	0.7418
Evaluation results	F	F	T	T	T	T	T	T
$(\gamma_d-\gamma)/\gamma_{d(\%)}$	–	–	10.36	8.36	8.14	15.42	11.85	6.61

T, with trend shift; F, without trend shift

landslide (tr) and the displacement rate of soil slope ($\dot{\varepsilon}$) as follows:

$$\log \mathrm{tr} = 2.33 - 0.516 \log(\dot{\varepsilon}) \pm 0.59 \quad (2)$$

The displacement rate ($\dot{\varepsilon}$) can be also expressed as follows:

$$\dot{\varepsilon} = \frac{\Delta l}{l \Delta t} \quad (3)$$

l distance between a back point and a front point (m); Δl relative displacement between two points (mm); Δt monitoring time (min).

When a slope enters the stage of accelerated deformation, the prediction of landslide can be made in terms of the curve of displacement–time and the empirical equation 2.

The statistical principle for the double-parameter threshold

If the monitoring points are independent of each other, the displacement velocities and the displacement vector angles (X_i) of the different monitoring points distributed on the same parent slope should follow the same normal distribution and have the same variance (σ). The sample mean ($\bar{X}$), the sample variance (S^2_{n-1}) and the sample statistical variance (q^2_{n-1}) are as follows:

$$\bar{X} = \frac{1}{n}\sum_{i=1}^{n} X_i \quad (4)$$

$$S^2_{n-1} = \frac{1}{n-1}\sum_{i=1}^{n} (X_i - \bar{X})^2 \quad (5)$$

$$q^2_{n-1} = \frac{1}{2(n-1)}\sum (X_{i+1} - X_i)^2 \quad (6)$$

According to the basic principle of statistics, when the locations of monitoring points have no evidence of change in time, S^2_{n-1} and q^2_{n-1} are the estimation of the variance (σ^2). Therefore their values should be almost the same. If all the points are gradually shifting and the variance (σ^2) is unchanged, the value of S^2_{n-1} will become larger just because of this trend's influence. Because q^2_{n-1} includes only the difference between the former monitoring value and the latter monitoring value, and eliminates most of the effect of the whole trend shift, the change in q^2_{n-1} is very little. A statistical variable (γ) can be used as the criterion for trend shift. It can be established as follows to verify whether there is a shift or not:

$$\gamma = \frac{q^2_{n-1}}{S^2_{n-1}} \quad (7)$$

Using a confidence level ($1-\alpha = 0.95$) and the threshold value of γ_d corresponding to ($\gamma_d = \bar{\gamma} + \frac{\sigma}{\sqrt{n}} Z_{0.025}$), supposing $\alpha = 0.05$, then calculate the value of γ_i by means of monitoring values. Finally, check the values of γ_i. If $\gamma_i \geqslant \gamma_d (\gamma_i = \gamma_1, \gamma_2, \ldots, \gamma_n)$, there is no trend shift by the confidence level α; if $\gamma_i < \gamma_d (\gamma_i = \gamma_1, \gamma_2, \ldots, \gamma_n)$, the slope has a trend shift.

It can be inferred that a trend shift in the displacements and vector angles of the slope will exist when that slope evolves into the overall sliding stage. A trend shift means evident change in the displacements and vector angles of a slope. This trend shift must lead to the trend shift of the statistical displacement velocity parameter γ (v) and the statistical displacement vector angle parameter γ (θ). However, in a stable slope, there is no trend shift in its displacement velocity or in the displacement vector angle. Thus, based on the principle above, the double-parameters forecast threshold for slope stability can be established as follows:

(1) If $\begin{cases} \gamma(\theta) < \gamma_d(\theta) \\ \gamma(v) < \gamma_d(v) \end{cases}$ then the slope goes into the overall sliding stage; a landslide may occur soon.

(2) If $\begin{cases} \gamma(v) \geqslant \gamma_d(v) \\ \gamma(\theta) < \gamma_d(\theta) \end{cases}$ or $\begin{cases} \gamma(v) < \gamma_d(v) \\ \gamma(\theta) \geqslant \gamma_d(\theta) \end{cases}$ then the slope is not stable, but a landslide is not likely to occur soon.

(3) If $\begin{cases} \gamma(\theta) \geqslant \gamma_d(\theta) \\ \gamma(v) \geqslant \gamma_d(v) \end{cases}$ then the slope is stable and there is little possibility of a landslide.

The trend displacement analysis and stability evaluation on Xintan slope by means of the double-parameter threshold

Based on the original monitoring data of F1–F8 points from July 2, 1984 to June 11, 1985 (Table 3)the displacement velocities and the surface displacement vector angles of the F-series points (Tables 4, 5), a systematic statistical analysis on the displacement velocity and the vector angles of the F-series monitoring points was carried out. The trend velocity statistical parameter γ_i (v), the statistical parameter γ_i (θ) of the trend displacement vector angle, the velocity statistical threshold γ_d (v) and the statistical threshold γ_d (θ) of the trend displacement vector angles were also determined. Using the double-parameter threshold of stability, evaluation results are shown in Tables 7 and 8.

From the double-parameter results (Tables 7, 8), both the velocities and the displacement vector angles of the F-series points on Xintan slope had a trend shift

before July 11, 1985. The slope was in a sliding state and the landslide was imminent. The calculated result coincided with the destabilized timetable of the Xintan landslide.

Conclusions

From the analysis above, the following conclusions can be drawn:

(1) The whole stability and response to the load in large accumulation landslides are affected and controlled by many factors. It is difficult to evaluate the stability and the sliding stage accurately by means of only a single parameter such as velocity or displacement. A new prediction theory for landslides using double parameters of the displacement vector angle and the displacement velocity to evaluate and describe the stability of a slope is proposed. Statistically, this new evaluation method overcomes limitations of the traditional displacement–time series analysis and forecast method, which considers only the deformation velocity.

(2) Variations of the surface displacement vector angles are essentially a comprehensive reflection of the stress and the different natural deformations of the slope, which inevitably reflect both stability state and slip evolvement. Therefore, the vector angle is an important parameter for describing slope stability, a parameter for which there can be no substitute.

(3) During development from the initial creeping deformation stage to the sliding stage, the surface displacement vector angles in the compressive shearing outlet decreases, but the displacement vector angles of the extension region of the back margin increases. The displacement vector angles of the flat sliding region are affected and controlled by the curve ratio of the sliding plane.

(4) The double-parameter criteria of displacement velocity and vector angles are statistically established, and evaluation and forecast for the stability of the Xintan slope in China was performed for verification. The double-parameter criteria is this: if the velocity and the vector angle both show a trend shift, the slope is entering the whole sliding stage. If the displacement vector angles have a trend shift but the velocity does not have a trend shift, the slope is in the initial stage of sliding. If neither the displacement velocity nor the vector angles have a trend shift, the slope is in a stable state.

(5) Stability of a slope was evaluated using double-parameter criteria based on actual displacement data of the F-series monitoring points on the Xintan slope. The results agree with the actual timetable of the landslide, and clearly show that the double-parameter criteria for stability of a slope has both precision and practicality in the evaluation of colluvial landslides.

(6) The methodology in this paper has been only applied to the typical colluvial landslide in Xintan landslide, China. If this methodology is going to be applied to other types of landslides, it still needs to be studied further.

Acknowledgments The study was supported by National Natural Science Foundation of China (40472141) and National Science Foundation of Shandong Province (Y2003E01). The authors would like to offer great thanks to Prof. Sun Guangzhou, Institute of Geology, Chinese Academy of Science, and Prof. Li Tiehan, China University of Geosciences, Beijing, for supplying the practical monitoring data of the Xintan slope. Postgraduates Wang Ronglu, Liuyan and Taojin have done much significant work on the monitoring and data analysis for this study.

References

Adib ME (2000) Slope failure in weathered claystone and siltstone. J Geotech Geoenviron Eng 126:787–792

Brand EW (1981) Some thoughts on rain-induced slope failure. In: Proceedings of the 10th international conference on soil mechanics and foundation engineering, Londen, vol 3, pp 374–376

Chen WF, Chan SW (1984) Upper bound limit analysis of the stability of seismic-informed earthslope. International symposium on geotechnical aspect of mass and material transportation, Bangkok, pp 284–286

Chen M, Wang L (1992) Grey forecasting on slope deformation and failure. In: Proceedings of the 29th international geological congress, Tokyo, pp 870–871

Chen L, Zhang M (1986) Major landslides along the Yangtze River, China. In: Abstract, AEG National Meeting, San Francisco, p 46

Liu G (1988) Environmental geologic investigation of Xintan landslide. Environ Geol Water Sci 12(1):11–13

Mair RJ (1993) Developments in geotechnical engineering research. In: Application to tunnels and deep excavation. In: Proceedings of the institution of civil engineers, London, vol 93, pp 30–37

Santian GE (1980) Landsliding. Falling and prevention. Science Press of China, pp 71–89

Savage WZ (1986) A model of the plastic flow of landslides. Geological Survey of America, Washington, pp 21–29

Wang S (1999) Monitoring and forecast of the landslides in three Gorge region of the Yangtze River. Geological Press, Beijing, pp 32–84

Wang LS, Zhang ZY, Zhan Z, Chen MD, Wei CQ, Han ZS (1988) On the mechanism of starting, sliding and braking of Xintan landslide in Yangtze Gorge. In: Proceedings of the 5th international symposium on landslides, Lausanne, Switzerland, pp 341–344